

# Modeling of Finite Gradient Elasticity Using Optimal Transportation Method

Boris JALUŠIĆ<sup>\*</sup>, Christian WEIBENFELS<sup>+</sup>,  
Jurica SORIĆ<sup>\*</sup>, Peter WRIGGERS<sup>+</sup>

<sup>\*</sup>*Faculty of Mechanical Engineering and Naval Architecture, University of Zagreb,  
Ivana Lučića 5, 10000 Zagreb, Croatia.  
E-mails: [boris.jalusic, jurica.soric](mailto:boris.jalusic@fsb.hr)@fsb.hr*

<sup>+</sup>*Institut für Kontinuumsmechanik, Leibniz Universität Hannover,  
Appelstraße 11, 30167 Hannover, Germany.  
E-mail: [weissenfels, wriggers](mailto:weissenfels@ikm.uni-hannover.de)@ikm.uni-hannover.de*

## **Abstract.**

*A meshfree Optimal Transportation Method (OTM) is applied for modeling of gradient hyperelasticity using higher-order theory based on only one microstructural parameter. The OTM method is utilized for the purpose of structural behaviour modeling undergoing large deformation. The independent displacement variables are approximated using interpolating maximum-entropy functions. This enables the satisfaction of the boundary conditions in a simple and straightforward manner without the need for the calculation of additional parameters. Novel stabilization algorithm employing one material point is presented. The analysis of numerical performance of the proposed approach is demonstrated by a representative numerical benchmark example. The obtained results are commented and arisen numerical problems are discussed.*

## **1 Introduction**

At the moment, a wide variety of different meshfree methods are being employed for modeling of various engineering problems. The reason behind this application are benefits and advantages in comparison with standard mesh-based methods, like Finite Element Method (FEM) [1]. The meshless numerical approaches are able to overcome problems such as element distortion and time-demanding mesh generation process. Nevertheless, the numerical integration and calculation of meshfree shape functions and its derivatives still represent a major task due to the associated high computational costs [2]. In the present contribution the OTM formulation [3] is adapted for modeling of deformation of homogeneous structures employing strain gradient elasticity theory [2]. In addition, the strain gradient elasticity based on the theory with only one microstructural parameter is considered. The gradient theory is utilized in order to more accurately capture the material behaviour, to remove discontinuities from strain and stress fields and to simulate the size effects. Size effects depend on the microstructure of the material and can be observed when the size of the specimen is sufficiently small, i.e. approximately the size of the microstructure. At this length scale, specimens with similar shape but different dimensions show different mechanical behaviors. The solution of fourth-order differential equations arising in considered theories requires a high-order continuity of approximation functions. Hence, using the FEM for solving this

type of problems is not a wise choice since standard formulations need to possess  $C^1$  continuity, which leads to complicated shape functions with large number of nodal degrees of freedom [4], even if mixed elements are utilized [5]. In comparison, the required continuity in the meshfree methods is obtainable in a simple by adding more nodes within the approximation domain [6].

The applied OTM method is based on the combination of the optimal transportation theory [7] with material-point sampling using the max-entropy meshless approximation [8]. It enforces the mass transport and essential boundary conditions exactly and should be free from tension instabilities. Furthermore, the method conserves linear and angular momentum [3]. The investigated global domain is approximated with two different sets of points, the discretization nodes and material points. At the nodes the displacements as the primary variables are computed by solving the discretized equation of motion. On the other hand, at the material points data associated with material is determined. This includes density, strain, stress, second-order stress, etc. Furthermore, the material points are used as integration points. The algorithms are based on the explicit time integration. In every time step the position of discretization points and the material points is calculated using updated Lagrangian scheme. The OTM algorithm is combined with the standard meshfree search algorithm where an arbitrary number of nodes can be assigned to a material point. Thus, the shape functions can become highly nonlinear if a larger number of nodes are located within the approximation domain. For the integration of the governing equations only one material point is used as in the originally proposed paper [3] to lower the computational time effort. It has been observed that one point is enough when solving the problem using classical continuum theory [9], but not might be when non-local (higher-order) continuum equations is employed. Hence, currently the novel stabilization algorithm using penalty method similar to one in [9] is being developed that could alleviate the methods stability issues.

The OTM framework for the modeling of deformation responses of homogeneous material using gradient elasticity is presented and explained at large in Section 2. Herein, the considered stabilization algorithm is also presented. In Section 3. the proposed stabilization algorithm is tested on a problem of the truss subjected to tensile test using uniform displacements at both ends. In Section 4 concluding remarks and further research guidelines are given.

## 2 Optimal Transportation Method for Finite Gradient Elasticity

### 2.1 Governing equations for a higher-order nonlinear continuum

The three dimensional higher-order nonlinear continuum which occupies the global computational domain  $\Omega$  surrounded by the global outer boundary  $\Gamma$  is considered. According to [10], the governing equation is the weak form of the dynamic equilibrium written as

$$\int_V \boldsymbol{\eta} \text{Div}(\text{Div} \mathbf{Q}) dV - \int_V \boldsymbol{\eta} \text{Div} \mathbf{P} dV - \int_V \boldsymbol{\eta} \rho \mathbf{b} dV + \int_V \boldsymbol{\eta} \rho \ddot{\boldsymbol{\phi}} dV = 0, \quad (1)$$

where  $\rho$  is the density and  $\ddot{\boldsymbol{\phi}}$  defines the second-order time derivative of deformation map (position vector  $\boldsymbol{\phi}(\mathbf{X}, t) = \mathbf{x}$  in the current configuration) defined as

$$\ddot{\boldsymbol{\phi}} = \frac{\boldsymbol{\phi}_{n-1} - 2\boldsymbol{\phi}_n + \boldsymbol{\phi}_{n+1}}{(\Delta t)^2}. \quad (2)$$

Furthermore, the displacement vector is defined and calculated as  $\mathbf{u}(\mathbf{X}, t) = \boldsymbol{\phi}(\mathbf{X}, t) - \mathbf{X}$ . In relation (1)  $\boldsymbol{\eta}$  denotes the admissible test function,  $\mathbf{P}$  the Piola stress tensor and  $\mathbf{Q}$  the double stress tensor. The tensors  $\mathbf{P}$  and  $\mathbf{Q}$  are defined as the partial derivatives of free energy density  $W = W^P(\mathbf{F}) + W^Q(\mathbf{G})$ . The free energy density is dependent on the first-order deformation gradient  $\mathbf{F} = \nabla_{\mathbf{x}} \boldsymbol{\phi}$  and the second-order deformation gradient  $\mathbf{G} = \nabla_{\mathbf{x}} \nabla_{\mathbf{x}} \boldsymbol{\phi}$ . Thus, the second- and third-order stress tensors are computed as

$$\mathbf{P} = \frac{\partial W}{\partial \mathbf{F}}, \quad \mathbf{Q} = \frac{\partial W}{\partial \mathbf{G}}. \quad (3)$$

The utilized free energy density function corresponds to the Neo-Hooke material used in [11] and is taken as

$$W^P(\mathbf{F}) = \frac{1}{2} \lambda \ln^2 J + \frac{1}{2} \mu (\mathbf{F} : \mathbf{F} - 3 - 2 \ln J), \quad (4)$$

$$W^Q(\mathbf{G}) = \mu l^2 \mathbf{G} : \mathbf{G}, \quad (5)$$

where  $\lambda$  and  $\mu$  denote the Lamé's constants,  $J$  the determinant of  $\mathbf{F}$  and  $l$  the parameter associated with the size of the microstructure of the higher-order continuum. In order to derive the appropriate equation to discretize the relation (1) is firstly integrated by parts (the first part two times), after that the divergence theorem is applied and the decomposition of the gradient operator is done to properly identify the higher-order boundary conditions [10] associated with the used continuum leading to

$$\int_V \mathbf{Q} : \nabla_{\mathbf{x}} (\nabla_{\mathbf{x}} \boldsymbol{\eta}) dV - \int_{\Gamma} \boldsymbol{\eta} \cdot \mathbf{t}^P d\Gamma - \int_{\Gamma} \nabla_{\mathbf{x}}^n \boldsymbol{\eta} \cdot \mathbf{t}^Q d\Gamma - \int_V \boldsymbol{\eta} \rho \mathbf{b} dV + \int_V \boldsymbol{\eta} \rho \ddot{\boldsymbol{\phi}} dV = 0, \quad (6)$$

where  $\mathbf{t}^P$  and  $\mathbf{t}^Q$  represent the standard traction vector and the higher-order traction vector, respectively. The weak form in (6) has to fulfill the essential boundary conditions

$$\mathbf{u} = \bar{\mathbf{u}}, \quad (7)$$

$$\nabla_{\mathbf{x}}^n \mathbf{u} = \nabla_{\mathbf{x}}^n \bar{\mathbf{u}}, \quad (8)$$

and natural boundary conditions

$$\mathbf{t}^P = (\mathbf{P} - \text{Div}\mathbf{Q}) \cdot \mathbf{N} + (\nabla_x \mathbf{N} \cdot (\mathbf{I} - \mathbf{N} \otimes \mathbf{N}) : \mathbf{I}) \cdot \mathbf{Q} : (\mathbf{N} \otimes \mathbf{N}) - (\nabla_x (\mathbf{Q} \cdot \mathbf{N}) \cdot (\mathbf{I} - \mathbf{N} \otimes \mathbf{N})) : \mathbf{I} = \bar{\mathbf{t}}^P \quad (9)$$

$$\mathbf{t}^Q = \mathbf{Q} : (\mathbf{N} \otimes \mathbf{N}) = \bar{\mathbf{t}}^Q, \quad (10)$$

outer boundary  $\Gamma$ .

## 2.2 Optimal Transportation Meshfree algorithm

In comparison to classical meshfree methods like Element Free Galerkin (EFG) [12] method not only the position of nodes but also the positions of material points are updated during calculation within the updated Lagrangian framework. In this contribution the OTM algorithm is derived using the central difference time integration scheme (2) in the presented weak form (6). Furthermore, the domain around each material point is defined as a support (integration) domain using the appropriate search algorithm. At every material point the test function  $\boldsymbol{\eta}$  and the deformation map  $\boldsymbol{\phi}$  are approximated using the max-entropy shape functions [8] and nodal values

$$\boldsymbol{\eta}_{pn} = \sum_{I=1}^{N_{pn}^{\text{sup}}} N_I(\mathbf{x}_{pn}) \boldsymbol{\eta}_I, \quad \boldsymbol{\phi}_{pn} = \sum_{I=1}^{N_{pn}^{\text{sup}}} N_I(\mathbf{x}_{pn}) \boldsymbol{\phi}_I. \quad (11)$$

Herein  $N_{pn}^{\text{sup}}$  is the number of nodes in the current support domain for each material point. Using the approximations (11) equation (6) is transformed to an algebraic equation

$$\frac{1}{(\Delta t)^2} \mathbf{M}_n \cdot \Delta \boldsymbol{\phi}_I^{n+1} = \mathbf{F}_n + \mathbf{G}_n + \mathbf{P}_n^P + \mathbf{P}_n^Q + \mathbf{R}_n + \frac{1}{(\Delta t)^2} \cdot \Delta \boldsymbol{\phi}_I^n. \quad (12)$$

In relation (12) the increments used are defined as  $\Delta \boldsymbol{\phi}^{n+1} = \boldsymbol{\phi}^{n+1} - \boldsymbol{\phi}^n$  and  $\Delta \boldsymbol{\phi}^n = \boldsymbol{\phi}^n - \boldsymbol{\phi}^{n-1}$ . The standard and higher-order forces at the outer boundary are given as  $\mathbf{P}_n^P$  and  $\mathbf{P}_n^Q$ , equal to

$$\mathbf{P}_n^P = \bigcup_{p=1}^{n_{mp}} \sum_{I=1}^{N_{pn}^{\text{sup}}} N_I(\mathbf{x}_{pn}) \cdot \bar{\mathbf{t}}^P \cdot \nu_{pn}, \quad (13)$$

$$\mathbf{P}_n^Q = \bigcup_{p=1}^{n_{mp}} \sum_{I=1}^{N_{pn}^{\text{sup}}} N_I(\mathbf{x}_{pn}) \cdot \mathbf{N} \cdot \bar{\mathbf{t}}^Q \cdot \nu_{pn}, \quad (14)$$

while the global mass matrix  $\mathbf{M}_n$  and residual vectors  $\mathbf{R}_n$ ,  $\mathbf{F}_n$  and  $\mathbf{G}_n$  are

$$\mathbf{M}_n = \bigcup_{p=1}^{n_{mp}} \sum_{I=1}^{N_{pn}^{\text{sup}}} \sum_{J=1}^{N_{pn}^{\text{sup}}} N_I(\mathbf{x}_{pn}) \cdot \mathbf{I} \cdot N_J(\mathbf{x}_{pn}) \cdot m_p, \quad (15)$$

$$\mathbf{R}_n = \bigcup_{p=1}^{n_{mp}} \sum_{I=1}^{N_{pn}^{\text{sup}}} N_I(\mathbf{x}_{pn}) \cdot \mathbf{b} \cdot m_p, \quad (16)$$

$$\mathbf{F}_n = - \bigcup_{p=1}^{n_{mp}} \sum_{I=1}^{N_{pn}^{\text{sup}}} \mathbf{B}_I(\mathbf{x}_{pn}) \cdot \mathbf{P} \cdot v_{pn}, \quad (17)$$

$$\mathbf{G}_n = - \bigcup_{p=1}^{n_{mp}} \sum_{I=1}^{N_{pn}^{\text{sup}}} \mathbf{H}_I(\mathbf{x}_{pn}) : \mathbf{Q} \cdot v_{pn}. \quad (18)$$

In relations (13) - (18) the  $m_p$  represents the mass and  $v_{pn}$  the volume at each material point. The matrices  $\mathbf{B}_I$  and  $\mathbf{H}_I$  contain the first- and second-order derivatives of the shape functions of node  $I$ . By solving (12) the incremental position vector  $\Delta\boldsymbol{\varphi}_I^{n+1}$  is determined and the nodal position vector is updated

$$\boldsymbol{\varphi}_I^{n+1} = \boldsymbol{\varphi}_I^n + \Delta\boldsymbol{\varphi}_I^{n+1}. \quad (19)$$

Furthermore, in order to reduce the computational time the lumped mass concept [13] within the OTM framework is utilized.

### 2.3 Stabilization procedure

For the purpose of preserving the same computational time and increasing the accuracy of the method the novel stabilization procedure is proposed. The procedure is based on method of penalizing the negative effects resulting from underintegration [14]. The developed stabilization algorithm is based on the assumption of only quadratic distribution of displacements within the influence domain. This is done by computing the normalized error at every material point inside the influence domain. The calculated error is then multiplied with the appropriate penalty parameter  $\varepsilon$  and subtracted from the nodal residual vector  $\mathbf{r}_I$  assembled analogously using the vectors  $\mathbf{R}_n$ ,  $\mathbf{F}_n$  and  $\mathbf{G}_n$  but utilizing the material points within the domain of influence. The normalized error criterion for every point  $p$  within the influence domain of the node  $I$  is

$$\mathbf{e}_{Ip} = \frac{d\mathbf{x} - d\tilde{\mathbf{x}}}{\|d\mathbf{X}\|} = \frac{(\mathbf{x}_{In} - \mathbf{x}_{pn}) - (\tilde{\mathbf{x}}_{In} - \tilde{\mathbf{x}}_{pn})}{\|\mathbf{X}_{In-1} - \mathbf{X}_{pn-1}\|}, \quad (20)$$

where the distance vectors calculated from the OTM method are defined as

$$\tilde{\mathbf{x}}_{ln} - \tilde{\mathbf{x}}_{pn} = \mathbf{F}_{pn} (\mathbf{X}_{ln-1} - \mathbf{X}_{pn-1}) + \mathbf{G}_{pn} : \left[ (\mathbf{X}_{ln-1} - \mathbf{X}_{pn-1}) \otimes (\mathbf{X}_{ln-1} - \mathbf{X}_{pn-1}) \right]. \quad (21)$$

In order to enforce the error to be zero the penalty method is applied and the stabilized nodal residual vector is computed as

$$\mathbf{r}_{ln}^{\text{stab}} = \mathbf{r}_{ln} - \varepsilon \sum_{p=1}^{N_l^{\text{inf}}} N_{ln}(\mathbf{x}_{pn}) \mathbf{e}_{lpn}. \quad (22)$$

### 3 Numerical example

#### 3.1 Truss subjected to large displacements

A three-dimensional truss subjected to mixed boundary conditions as shown in Figure 2 is considered. The truss is subjected to large displacements at the front and back side, while the other components of boundary conditions are the standard tractions and higher-order traction which are taken as zero. The geometry of the truss is defined by the length  $L=1$ . For the analysis of deformation the benchmark material properties of the truss are taken as  $E=1 \cdot 10^6$ ,  $\nu=0.3$  and  $\rho=1 \cdot 10^6$ . The large density is chosen here in order to compute the example faster in a quasi-static case to test the stabilization algorithm for the higher-order continuum. For the purpose of comparing the solutions, firstly the deformation of the geometrically identical truss under the assumption of the classical continuum without any microstructural effects included is computed. In Figures 3 and 5, the deformed shapes of the truss with the contours of the displacements in the z direction and the Von Mises stress are shown. As seen from the deformed shape in Figure 3, the truss at both ends reached the final values of the displacement boundary conditions.

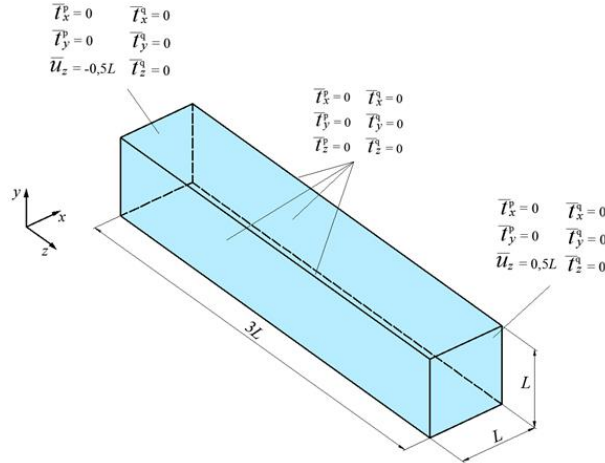


Figure1: Truss with boundary conditions

Secondly, a higher-order continuum with a very small value of the microstructural parameter of  $l/L=0.05$  is applied in computations. Here it should be mentioned that by introducing the higher-order continuum and within that the calculation of second-

order derivatives, no solution can be achieved without the application of stabilization procedure. Hence, the under integration of the weak form has a very large effect on the deformation of the structure, numerical calculations can not be performed because of very large errors arising during computation process.

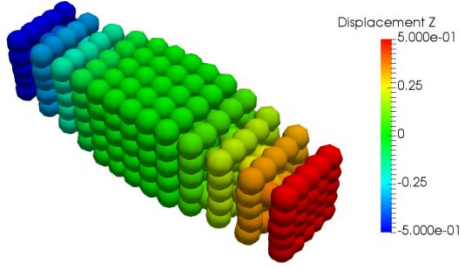


Figure2: Truss – classical continuum – distribution of displacement  $u_z$

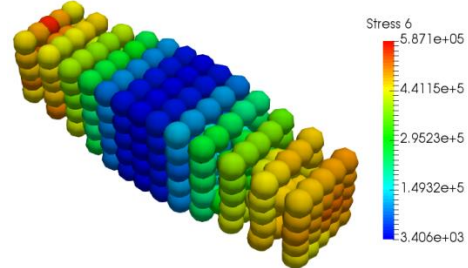


Figure4: Truss – classical continuum – distribution of Von Mises stress

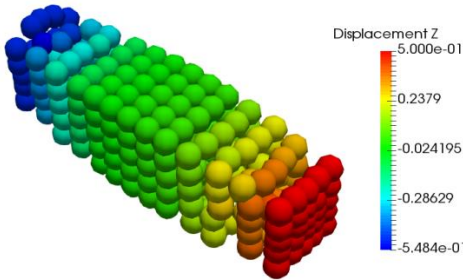


Figure3: Truss – higher-order continuum – distribution of displacement  $u_z$

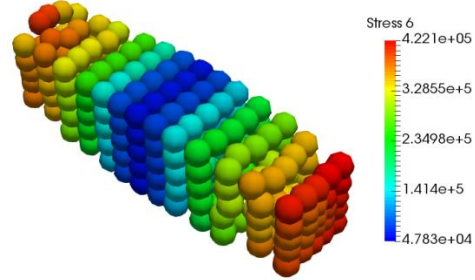


Figure5: Truss – higher-order continuum – distribution of Von Mises stress

In Figures 3 and 5, the obtained deformed shapes of the higher-order continuum with very high value of the stabilization parameter are portrayed. By the final positions of the nodes, it is clear that the application of the presented stabilization procedure causes the destruction of the displacement boundary conditions and deformed continuum forms which are not accurate. Hence, here additional numerical studies are necessary in order to determine why the mentioned problems persist. Furthermore, as an alternative to max-entropy approximation functions different more robust approximation functions should be taken in consideration and the obtained results should be compared.

#### 4 Conclusion

The meshfree OTM formulation has been applied for the modeling of deformation of the homogeneous structure. The influence of the material microstructure is taken into account using one parameter within the free energy density of the utilized higher-order continuum. Furthermore, as a remedy to the methods stability issues connected to underintegration of the weak form novel stabilization procedure is employed. The OTM algorithm is tested on one benchmark truss example. Using the presented stabilization algorithm, solutions can be obtained, however some problems have been identified. The first problem is the determination of the value of the penalty parameter if higher-order

continuum is computed. It is really hard to choose the value of the penalty due to the incorrect integration of the second-order derivatives of the max-entropy shape functions that are complex and their values is not easy to control. The second problem observed is that the stabilization procedure destroys the essential boundary conditions. In further research the mentioned issues should be addressed. The change to the more robust approximation functions should be considered. This could improve the smoothness of second-order derivatives and more accurate calculations should be carried out.

**Acknowledgement:** This work has been supported in part by Croatian Science Foundation under the project 2516. The investigations are also a part of the project supported by Alexander von Humboldt Foundation.

## References

- [1] P. Wriggers, *Nonlinear Finite Element Methods*, Springer Science & Business Media 2008.
- [2] H. Askes, E.C. Aifantis, Gradient elasticity in statics and dynamics: An overview of formulations, length scale identification procedures, finite element implementations and new results, *International Journal of Solids and Structures*, 48 (2011) 1962-1990.
- [3] B. Li, F. Habbal, M. Ortiz, Optimal transportation meshfree approximation schemes for fluid and plastic flows, *International Journal for Numerical Methods in Engineering*, 83 (2010) 1541-1579.
- [4] S.-A. Papanicolopoulos, A. Zervos, I. Vardoulakis, A three-dimensional C1 finite element for gradient elasticity, *International Journal for Numerical Methods in Engineering*, 77 (2009) 1396-1415.
- [5] E. Amanatidou, N. Aravas, Mixed finite element formulations of strain-gradient elasticity problems, *Computer Methods in Applied Mechanics and Engineering*, 191 (2002) 1723-1751.
- [6] Z. Tang, S. Shen, S.N. Atluri, Analysis of materials with strain-gradient effects: A Meshless Local Petrov-Galerkin (MLPG) approach, with nodal displacements only, *Cmes-Computer Modeling in Engineering & Sciences*, 4 (2003) 177-196.
- [7] C. Villani, *Topics in optimal transportation theory*, Graduate Studies in Mathematics, American Mathematical Society, Providence, Rhode Island, USA, 2003.
- [8] M. Arroyo, M. Ortiz, Local maximum-entropy approximation schemes: a seamless bridge between finite elements and meshfree methods, *International Journal for Numerical Methods in Engineering*, 65 (2006) 2167-2202.
- [9] C. Weißenfels, P. Wriggers, Stabilization algorithm for the optimal transportation meshfree approximation scheme, *Computer Methods in Applied Mechanics and Engineering*, 329 (2018) 421-443.
- [10] R. Sunyk, P. Steinmann, On higher gradients in continuum-atomistic modelling, *International Journal of Solids and Structures*, 40 (2003) 6877-6896.
- [11] P.E. Fischer, *C1 Continuous Methods in Computational Gradient Elasticity*, Universitat Erlangen-Nürnberg, Germany, 2011.
- [12] T. Belytschko, Y.Y. Lu, L. Gu, Element-free Galerkin methods, *International Journal for Numerical Methods in Engineering*, 37 (1994) 229-256.
- [13] L. Fedeli, A. Pandolfi, M. Ortiz, Geometrically-exact time-integration mesh-free schemes for advection-diffusion problems derived from optimal transportation theory and their connection with particle methods, 2017.
- [14] G.C. Ganzenmüller, An hourglass control algorithm for Lagrangian Smooth Particle Hydrodynamics, *Computer Methods in Applied Mechanics and Engineering*, 286 (2015) 87-106.